Design and Application of a Four-Channel Transmit/Receive Surface Coil for Functional Cardiac Imaging at 7T

Article *in* Journal of Magnetic Resonance Imaging · March 2011

DOI: 10.1002/jmri.22451 · Source: PubMed

13 authors, including:

Matthias Alexander Dieringer
Siemens
76 PUBLICATIONS **437** CITATIONS
SEE PROFILE

Tobias Frauenrath
University Hochschule Niederrhein
30 PUBLICATIONS **303** CITATIONS
SEE PROFILE

Helmar Waiczies
MRI.Tools GmbH
71 PUBLICATIONS **397** CITATIONS
SEE PROFILE

Jan Rieger
MRI.TOOLS GmbH
42 PUBLICATIONS **197** CITATIONS
SEE PROFILE

Technical Note

Design and Application of a Four-Channel Transmit/Receive Surface Coil for Functional Cardiac Imaging at 7T

Matthias A. Dieringer, MSc,[1–3]* Wolfgang Renz, PhD,[2,4] Tomasz Lindel, MSc,[2,5] Frank Seifert, PhD,[2,5] Tobias Frauenrath, PhD,[2] Florian von Knobelsdorff-Brenkenhoff, MD,[1–3] Helmar Waiczies, PhD,[2,5] Werner Hoffmann, PhD,[2,5] Jan Rieger, BSc,[2] Harald Pfeiffer, MSc,[2,5] Bernd Ittermann, PhD,[2,5] Jeanette Schulz-Menger, MD,[1–3] and Thoralf Niendorf, PhD[1,2]

Purpose: To design and evaluate a four-channel cardiac transceiver coil array for functional cardiac imaging at 7T.

Materials and Methods: A four-element cardiac transceiver surface coil array was developed with two rectangular loops mounted on an anterior former and two rectangular loops on a posterior former. specific absorption rate (SAR) simulations were performed and a B_1^+ calibration method was applied prior to obtain 2D FLASH CINE (mSENSE, R = 2) images from nine healthy volunteers with a spatial resolution of up to $1 \times 1 \times 2.5$ mm^3.

Results: Tuning and matching was found to be better than 10 dB for all subjects. The decoupling (S_{21}) was measured to be >18 dB between neighboring loops, >20 dB for opposite loops, and >30 dB for other loop combinations. SAR values were well within the limits provided by the IEC. Imaging provided clinically acceptable signal homogeneity with an excellent blood-myocardium contrast applying the B_1^+ calibration approach.

Conclusion: A four-channel cardiac transceiver coil array for 7T was built, allowing for cardiac imaging with clinically acceptable signal homogeneity and an excellent blood-myocardium contrast. Minor anatomic structures, such as pericardium, mitral, and tricuspid valves and their apparatus, as well as trabeculae, were accurately delineated.

Key Words: ultrahigh field cardiovascular MRI; RF coil design; left ventricular function; 7.0 Tesla; 7T cardiac imaging

J. Magn. Reson. Imaging 2011;33:736–741.

THE CLINICAL NEED for speed and efficiency dictated by physiological motion and flow constraints has been a significant motivating force for the development of ever more rapid cardiovascular magnetic resonance (CMR) imaging techniques and advanced magnetic resonance imaging (MRI) system hardware. Today, a move toward widespread availability of clinical high-field MR systems (B_0 = 3T) is under way. Another important development, which is on the CMR research horizon, is the move toward ultrahigh-field MR systems (B_0 = 7T) (1–6). However, ultrahigh-field CMR is regarded as one of the most challenging MRI applications. Image quality is not always exclusively defined by signal-to-noise ratio (SNR) and contrast-to-noise ratio (CNR). Practical obstacles are exacerbated conductive and dielectric effects in tissue, typically manifested in radiofrequency (RF) nonuniformities causing shading or local signal dropoff. Also, there are RF power deposition constraints due to local tissue heating. All of these detrimental effects bear the potential to spoil the benefit of CMR at 7T. Hence, the goal of this study was to overcome these problems by finding a strategy to enable CMR with clinically acceptable image quality by employing RF transmit/receive (also denoted as "TX/RX" or "transceiver") coil arrays dedicated for CMR. Recent designs for 7T transceiver torso coil arrays have typically been laid out as strip line elements on rigid or semiflexible frames (1). Other versions of 7T cardiac transceiver arrays used flexible designs consisting of a pair of four-element strip line arrays (2,7). Since multitransmit MR systems with eight and more channels are not widely available yet, comparatively simple cardiac coils have also been successfully used (4). The first objective of this study

[1]Experimental and Clinical Research Center (ECRC), Charite' University Medicine Campus Berlin Buch, Berlin, Germany.

[2]Berlin Ultrahigh Field Facility (B.U.F.F.), Max-Delbrueck-Center for Molecular Medicine, Berlin, Germany.

[3]Clinic for Cardiology and Nephrology, HELIOS Clinic Berlin Buch, Berlin, Germany.

[4]Siemens Healthcare, Erlangen, Germany.

[5]Physikalisch-Technische Bundesanstalt, Metrology in Medicine, Berlin, Germany.

*Address reprint requests to: M.A.D., Berlin Ultrahigh Field Facility, Max-Delbrueck-Centrum for Molecular Medicine, Robert-Roessle-Str. 10, D-13125 Berlin, Germany.
E-mail: Matthias.Dieringer@mdc-berlin.de

Received August 26, 2010; Accepted November 10, 2010.

DOI 10.1002/jmri.22451
View this article online at wileyonlinelibrary.com.

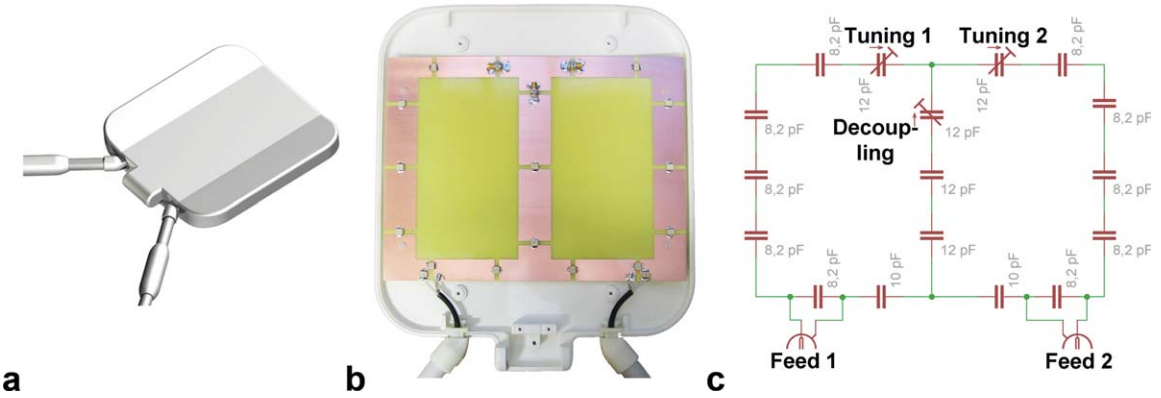

Figure 1. A rendered 3D model of one modestly curved lightweight coil casing former (**a**) together with the interior of the proposed coil design (**b**) and the basic circuit diagram (**c**). [Color figure can be viewed in the online issue, which is available at wileyonlinelibrary.com.]

was to design a cardiac optimized four-channel transceiver surface coil array configuration that uses loop elements, and that provides image quality suitable for clinical use, patient comfort, and ease of use. Finally, this study demonstrates the suitability of our setup for 2D CINE acquisitions and the assessment of left ventricular (LV) function in initial volunteer studies. The merits and limitations of the four-channel transceiver array are discussed, and implications for cardiac MR at 7T are considered.

MATERIALS AND METHODS

Coil Design

RF interference due to coupling of transmitting coil elements is disruptive at ultrahigh fields. An increased number of coil elements reduces the loop size, with which the unloaded-to-loaded-Q ratio decreases (8). Small loop sizes may result in limited B_1 penetration, but fewer elements, such as two, may have B_1^+/B_1^- twisting issues (9). Thus, we incorporated a limit of four elements in this first approach. Furthermore, a simple strategy to increase the coupling of the coil to the body was chosen by placing the coil as close as possible to the body (8) but leaving a distance of 1 cm to avoid exaggerated transmission surface coupling. The four coil loops were constructed on two modestly curved lightweight formers to conform to an average chest and back (Fig. 1a). Two rectangular loops were mounted each on the anterior and the posterior former (Fig. 1b). The loop size of a single coil loop element was set to 13 × 20 cm to enable whole heart coverage and appropriate depth penetration. Capacitive shortening was used extensively (Fig. 1c). Coil decoupling for neighboring loops was achieved by a common conductor with a shared decoupling capacitor (10). Decoupling between the anterior and posterior section is accomplished by the subject's body itself. Bench measurements for coil tuning/matching were performed on a Rhode & Schwarz ZVL Network Analyzer (Rhode Schwarz, Memmingen, Germany). To mitigate radiation losses, an RF screen made of thin slotted copper foil was positioned at the back side of the loop elements at a distance of 2 cm. Coaxial coil feeding was accomplished via baluns (sleeve type or "bazooka," capacitively shortened), one for each channel at a distance of 12 cm from the feeding point. The baluns were surrounded by foam sleeves to minimize the interaction with the environment. Noise correlation was measured in vivo on one volunteer.

MR Hardware

All images were acquired on a 7T whole body scanner (Siemens Healthcare, Erlangen, Germany) comprising a 90 cm bore magnet (Magnex Scientific, Oxfordshire, UK) equipped with a Siemens Avanto gradient system (slew rate: 200 T/m/s, max. gradient strength: 40 mT/m; Siemens Medical Solutions, Erlangen, Germany), and an 8 kW RF amplifier (Stolberg HF-Technik AG, Stolberg-Vicht, Germany). For B_1-mapping, four transmit channels of a TX-Array (Siemens Healthcare) were used. Since there is no monitoring system for the TX-Array available yet, the volunteer studies were performed with a single transmission channel. Therefore, each coil element was connected via an interface box containing T/R switches, low noise preamplifiers, and an RF power splitter/combiner to a single transmit channel configuration.

B_1 Calibration

While B_1^+ represents the transmit component of the RF magnetic field vector, B_1^- stands for the receive field component. B_1^+ shimming is used to reduce RF nonuniformities, to maximize B_1^+ coherence, and thus the excitation efficiency as well as SNR and contrast between different tissues for a given location in the body. One way to contrive B_1^+ shimming is to acquire relative B_1 maps (11). Therefore, four measurements were performed with each transmit coil element individually using the TX-Array, while all four coil elements were used for reception. To produce a reference image, all images were combined by the sum of squares approach. Since this reference image was influenced by both B_1^+ and B_1^- compounds, the received single-channel images were summed up by sum of squares for each transmit channel

individually. Using the approximation that the sum of squares of all transmit channels is uniform, the reference image was divided by this result to eliminate B_1^- contributions to achieve an appropriate target excitation profile. The needed transmit amplitudes were retrieved by solving $B_i \cdot C_i = M_i$, where B_i is the corresponding B_1^+ and $C_i = A_i \cdot e^{(i\psi_i)}$ (where A_i is the relevant amplitude, ψ_i is the corresponding phase) is the scale factor to achieve the desired pattern M_i. A Marquardt-Levenberg routine fitted the absolute values to minimize the term $|M_i| - |B_i \cdot C_i|$ for a given region of interest. The relative phases derived from the B_1-mapping routine of a water phantom, containing 1.33 g/L NaCl and 0.66 g/L $CuSO_4$ to mimic the load of a human torso, were incorporated into the setup used for the volunteer studies by adapting the cable length for each coil element. Volunteer specific B_1^+ shimming was not performed.

Specific Absorption Rate (SAR) Simulations

Power deposition varies approximately with the square of the frequency and thus with the square of the magnetic field strength. In the hypothetical case of an otherwise identical B_1^+ distribution, this means an increase by a factor of 22 when going from 1.5T to 7T. In reality, this factor is even aggravated by RF inhomogeneities at 7T. To achieve optimum flip angles at 7T and thus high tissue contrast while not putting the subject at any risk, we performed finite-differences time-domain (XFDTD 6.4, Remcom, State College, PA) simulations on a 201^3 mesh of $2 \times 2 \times 2$ mm^3 cells using a truncated body model ("Duke") from the Virtual Family dataset (IT'IS Foundation, Zurich, Switzerland (12)). Simulations were performed with 1) B_1^+ shimming, 2) B_1^- shimming, each with 3) positive and 4) negative phase order. Tissue dielectric properties for 300 MHz were used and the coil including feeding ports and capacitors was modeled in a tuned and decoupled configuration. For given driving conditions of the coil, the SAR distribution inside the body was calculated and power limits for safe operation were derived (13). B_1^+ values within the cardiac muscle were estimated using these simulations.

Sequence Design

A retrospectively gated 2D CINE FLASH (fast low angle shot) sequence (breathold scan; echo time = 2.7 msec; repetition time = 5.4 msec; voxel size = $(1.4\times1.4\times4)$ mm^3; matrix size = 256×186, temporal resolution = 49 msec; total scan time ~15 seconds including a delay of 3 seconds to offset SAR constraints, parallel imaging (R = 2) using the mSENSE approach, Siemens Healthcare) was used.

Cardiac Gating

In a high magnetic field, the recording of an electrocardiogram (ECG) is severely disrupted by the magneto hydrodynamic effect. This renders the conventional ECG triggering unsuitable at 7T. Therefore, we opted for a novel approach and used an acoustic cardio triggering/gating device (ACT (14,15)) for cardiac gating.

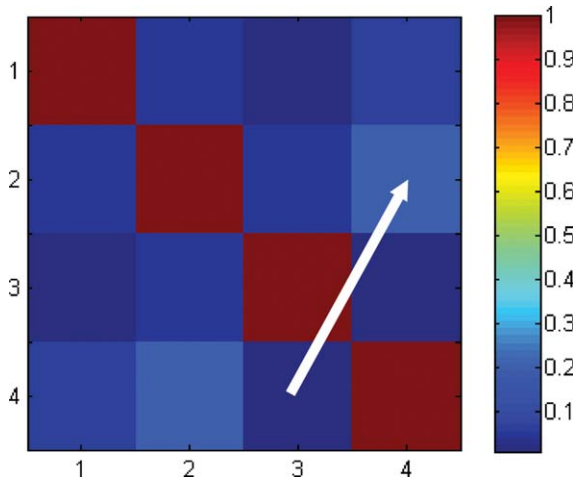

Figure 2. Noise correlation for the four loop elements measured in vivo. The highest value (white arrow) was 0.1997. [Color figure can be viewed in the online issue, which is available at wileyonlinelibrary.com.]

Volunteer Studies

The coil received approval for clinical studies by a certified body. MRI was performed in healthy adult male volunteers ($n = 9$, mean age 36 ± 10 years, range 27–52 years; mean body surface area 1.9 ± 0.1 m^2; range 1.75–2.04 m^2) only before extra variances due to gender and/or pathophysiological conditions were introduced. Informed written consent was obtained from each volunteer prior to the study, in compliance with the local Institutional Review Board guidelines. Three different cardiac views (short axis, four-chamber view, and two-chamber view) were acquired from each subject to assess the coil design. Cardiac chamber quantification was conducted using CMR42 (Circle CVi, Calgary, AB, Canada). Mean SNR estimates were determined as described previously (6).

RESULTS

Performance of the Transceiver Coil Array

The RF characteristics of the coil array as measured on the bench resulted in a decoupling (S_{21}) between neighboring loops of >18 dB (measured on the water phantom), a decoupling between opposite loops >20 dB, a decoupling between other coil element combinations >30 dB, and Q factors of 70 (unloaded) and 10 (loaded with a human body), respectively. The coil maintained a fixed tuning and matching that was found to be better than 10 dB (typically 13 dB) for all subjects. Coil loading did not vary greatly for the range of body mass index used. The weight of one coil segment is 1350 g. The measured noise correlation matrix is illustrated in Fig. 2.

SAR Simulations

The average output power of the RF amplifier was limited to 30W (6 minutes averaging period). The exposed mass of the torso, defined as the mass within the volume in which 95% of the total absorbed RF power is

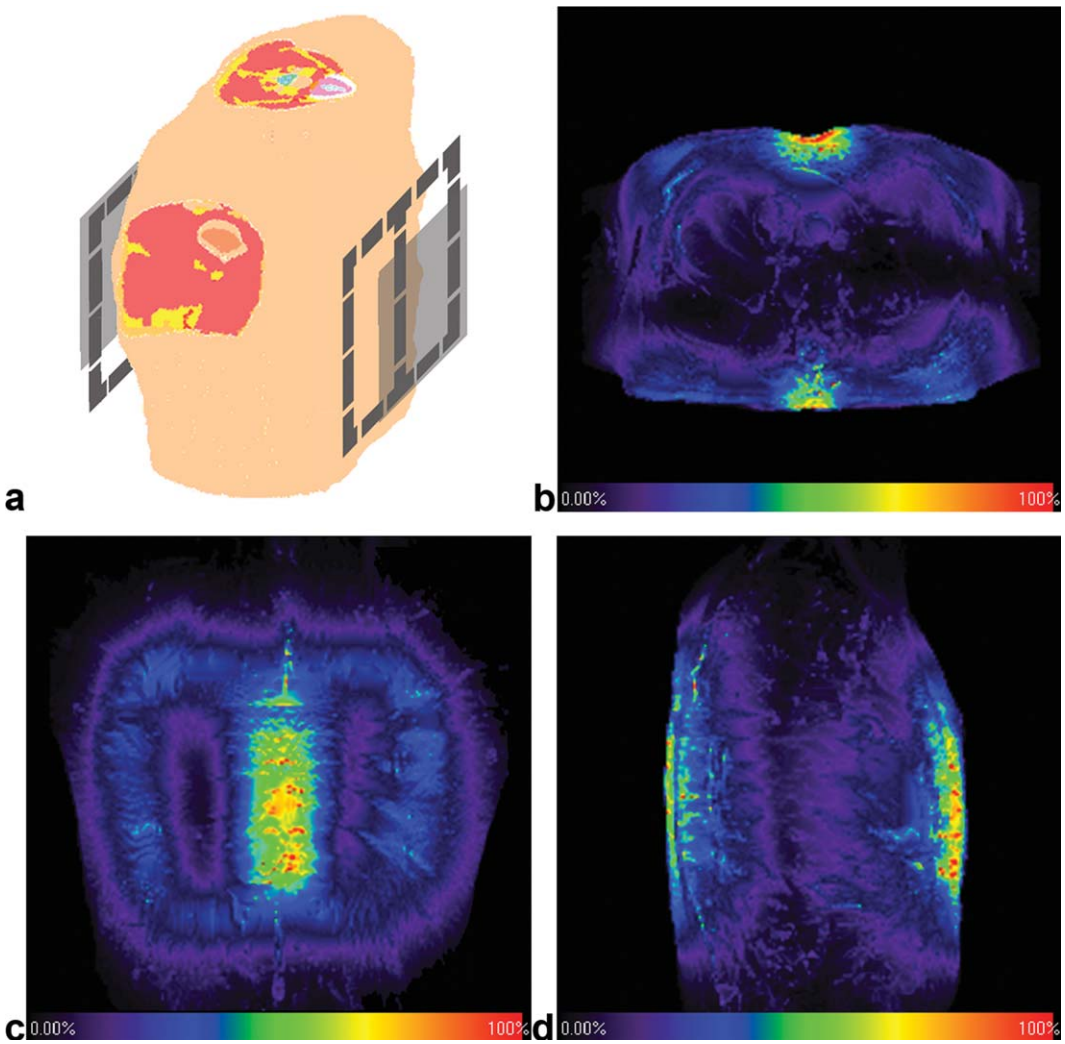

Figure 3. FDTD simulation setup with a truncated torso model (**a**). MIP of nonaveraged SAR distribution in a transversal (**b**), coronal (**c**), and sagittal (**d**) slice at 30W input power and best B_1^+ shim phase setting. The RF power deposition is scaled from 0 (black) to 42 W/kg (red), the corresponding maximum 10 g averaged SAR is 15.1 W/kg, partial body SAR is 1.4 W/kg.

deposited, was determined to be 19.8 kg. For any tested phase configuration, the corresponding partial body SAR, including radiation losses, did not exceed 1.4 W/kg. This is well within the limits of whole body SAR provided by the IEC 60601-2-33 (2 W/kg in normal mode, 4 W/kg in first level mode). The calculated local SAR (averaged over 10 g of tissue) was found to be 15.0–16.5 W/kg for the tested phase settings and thus did not exceed 20 W/kg, which is in compliance with the new IEC 60601-2-33 Ed.3. This is a conservative estimate since all losses in cables, switches, and the coil's RF components were ignored. The maximum intensity projections of the SAR calculations for each slice orientation within the optimum shimming set are depicted in Fig. 3. The estimated B_1^+ derived from the simulations ranged from 10 to 15 μT/square root of kW in the heart.

Cardiac Imaging

Results obtained with 2D CINE FLASH imaging using the 4-channel TX/RX coil array are depicted in Fig. 4. Images acquired without B_1^+ calibration are prone to severe inhomogeneities in the signal intensities embodied by dark regions in the myocardium or blood pool. B_1^+ calibrated images, on the other hand, provided a signal homogeneity, which is certainly not perfect yet, but can be considered clinically acceptable. CINE imaging provided excellent blood-myocardium contrast for all examined slice orientations in all of the nine volunteers, as shown in Fig. 5a. In contrast to 1.5T 2D CINE FLASH, the prolonged T_1 at 7T resulted in an improved contrast between myocardium and blood. This enhanced myocardium blood contrast exists not only for short axis views perpendicular to the blood flow but it was also observed for long axis views parallel to the flow. Minor anatomic structures such as pericardium, mitral and tricuspid valves, and their apparatus including papillary muscles and trabeculae are accurately identifiable.

In another example shown in Fig. 5b–e, the baseline SNR gain at 7T was translated into a reduction of the slice thickness, which was set to values as low as 2.5 mm while accomplishing a 1-mm^2 in-plane spatial

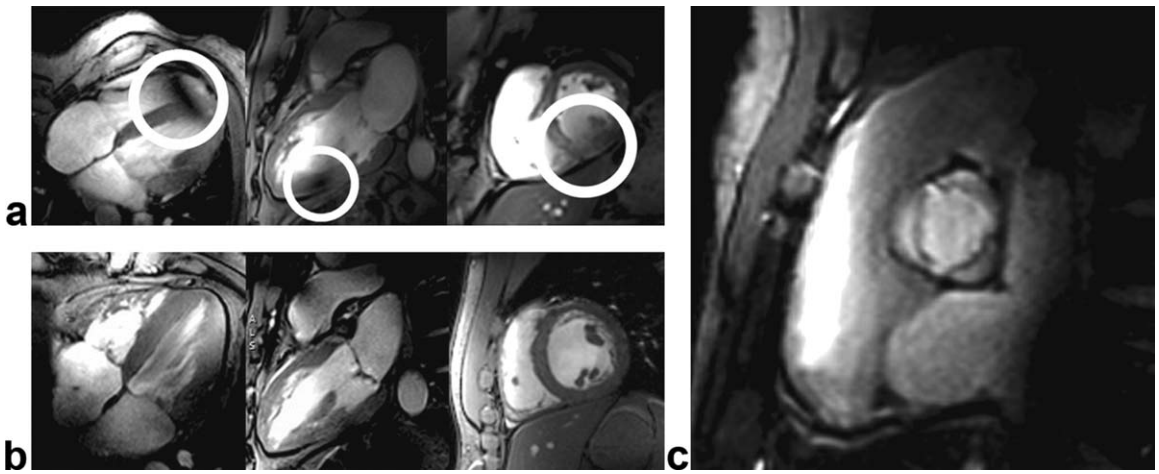

Figure 4. 2D FLASH CINE images acquired at late diastole without (**a**) and with B_1^+ calibration (**b**) following the approach described in Materials and Methods. While the images without B_1^+ calibration are affected by severe artifacts like dark spots (white circles), B_1^+ calibration significantly improved the signal uniformity across the desired region of interest, where ventricular blood and myocardium can be clearly differentiated. Valve structures, papillary muscles and trabeculae, as well as the aortic valve (**c**) are sharply delineated.

resolution. Cardiac chamber quantification using a slice thickness of 4 mm yielded an LV diastolic volume of 160.5 ± 12.8 mL, an LV systolic volume of 60.0 ± 6.6 mL, LV mass of 127.3 ± 9.2 g, and an ejection fraction of 62.7 ± 2.7%. An approximate SNR assessment provided mean SNR estimates including all subjects of SNR = 165 ± 25 for 7 mm slices (6).

DISCUSSION

The designed four-channel cardiac transceiver surface coil has the capability to acquire high contrast, high spatial and temporal resolution in vivo 2D CINE FLASH cardiac morphology images at 7T. The RF penetration seems sufficient for normal volunteers and B_1^+ nonuniformities can be mitigated with B_1^+ shimming. The inherent SNR benefit of ultrahigh-field MRI together with the SNR advantage of a closely fitting surface coil were transferred into cardiac function imaging. For this purpose the slice thickness was reduced to 4 mm with an in-plane spatial resolution as small as 1 mm^2, while CINE imaging at 1.5T usually applies a slice thickness ranging between 5–10 mm. The results demonstrate that cardiac morphology and functional imaging at 7T is possible. The limited number of coil elements may be prohibitive for larger acceleration factors due to coil geometry-related noise amplification, but an acceleration factor of two using the mSENSE approach is feasible. While this pilot study was aiming at a proof of concept, the close examination of the reliability and accuracy of LV function assessment at 7T and its benchmarking with cardiac function imaging (clinically established at 1.5T) is under way (6). The SAR simulations, as well as the in vivo acquisitions reported here illustrate the

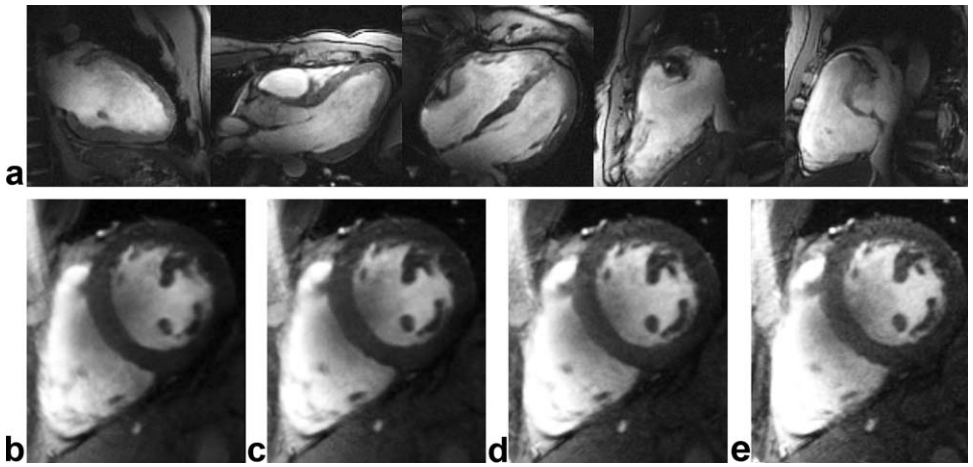

Figure 5. **a**: 2D FLASH CINE images acquired at early systole with the described B_1^+ shimming approach in various slice alignments (from left to right: two-chamber long axis view, three-chamber long axis view, four-chamber long axis view, long axis view of the right ventricle, aortic valve). Mid-cavity short axis views acquired with 2D FLASH CINE at diastole using the four-channel transmit/receive RF coil at 7T. The baseline SNR advantage at 7T was translated into a reduction of the slice thickness from (**b**) 8 mm, to (**c**) 6 mm, to (**d**) 4 mm, and to (**e**) 2.5 mm while achieving (1×1) mm^2 in-plane spatial resolution.

impediments of nonuniform B_1^+ distributions, which can be mitigated by B_1^+ shimming procedures. For this reason, various B_1^+ shimming procedures were proposed (16–19) and are currently being examined by numerous groups. Admittedly, a mismatch between the calculated SAR and the actual body SAR might remain. This is a general issue, which is part of the RF safety discussion and requires further investigation.

In conclusion, the outcome of this volunteer study renders our setup suitable for gaining uniform, high spatial and temporal resolution cine images with diagnostic image quality. The proposed B_1^+ calibration probably may not be suitable for all patient geometries. Hence, we anticipate expanding our work to a patient-based B_1^+ shimming routine to facilitate diagnostic images for a broader range of body geometries and body mass indices. Also, we anticipate comparing our four loop element TX/RX design with other designs such as the coils based on strip-lines structure, which is beyond the scope of the current study. As ultrahigh-field MR systems become more widespread, improvement in hardware, software, and MR methodology is expected to further improve image quality for 2D CINE and other CMR applications. The benefits of such improvements would be in positive alignment with the clinical needs of an ever-growing spectrum of indications for CMR. This involves a broad variety of cardiovascular disorders, including the detection and differentiation of ischemic and inflammatory disorders (20) or the noninvasive characterization of tissue changes.

REFERENCES

1. Vaughan JT, Snyder CJ, DelaBarre LJ, et al. Whole-body imaging at 7T: preliminary results. Magn Reson Med 2009;61:244–248.
2. Snyder CJ, DelaBarre L, Metzger GJ, et al. Initial results of cardiac imaging at 7 Tesla. Magn Reson Med 2009;61:517–524.
3. van Elderen SG, Versluis MJ, Webb AG, et al. Initial results on in vivo human coronary MR angiography at 7 T. Magn Reson Med 2009;62:1379–1384.
4. Versluis MJ, Tsekos N, Smith NB, Webb AG. Simple RF design for human functional and morphological cardiac imaging at 7tesla. J Magn Reson 2009;200:161–166.
5. Brandts A, Westenberg JJ, Versluis MJ, et al. Quantitative assessment of left ventricular function in humans at 7 T. Magn Reson Med 2010;64:1471–1477.
6. von Knobelsdorff-Brenkenhoff F, Frauenrath T, Prothmann M, et al. Cardiac chamber quantification using magnetic resonance imaging at 7 Tesla-a pilot study. Eur Radiol 2010;20:2844–2852.
7. Maderwald S, Orzada S, Schäfer LC, et al. 7T human in vivo cardiac imaging with an 8-channel transmit/receive array. In: Proc 17th Annual Meeting ISMRM, Honolulu; 2009 (abstract 822).
8. Wald LL, Wiggins G. New coil systems for highly parallel MR acquisition strategies. In: Schoenberg SO, Dietrich O, Reiser MF, editors. Parallel imaging in clinical MR applications, 12 ed. Medical Radiology-Diagnostic Imaging. Berlin, Heidelberg: Springer; 2007. p 497–510.
9. Duan Q, Sodickson DK, Lattanzi R, Zhang B, Wiggins GC. Optimizing 7T spine array design through offsetting of transmit and receive elements and quadrature excitation. In: Proc 18th Annual Meeting ISMRM, Stockholm; 2010 (abstract 51).
10. Wang J. A novel method to reduce the signal coupling of surface coils for MRI. In: Proc 14th Annual Meeting ISMRM, Seattle; 1996 (abstract 1434).
11. Ullmann P, Junge S, Seifert F, Wick M, Ruhm W, Henning J. Experimental analysis of parallel excitation using dedicated coil setups and simultaneous RF transmission on multiple channels. Magn Reson Med 2005;54:994–1001.
12. Christ A, Kainz W, Hahn EG, et al. The Virtual Family—development of surface-based anatomical models of two adults and two children for dosimetric simulations. Phys Med Biol 2010;55: N23–38.
13. Seifert F, Wubbeler G, Junge S, Ittermann B, Rinneberg H. Patient safety concept for multichannel transmit coils. J Magn Reson Imaging 2007;26:1315–1321.
14. Frauenrath T, Hezel F, Heinrichs U, et al. Feasibility of cardiac gating free of interference with electro-magnetic fields at 1.5 Tesla, 3.0 Tesla and 7.0 Tesla using an MR-stethoscope. Invest Radiol 2009;44:539–547.
15. Frauenrath T, Niendorf T, Kob M. Acoustic method for synchronization of magnetic resonance imaging (MRI). Acta Acustica united with Acustica 2008:148–155.
16. Brunner DO, Pruessmann KP. B1(+) interferometry for the calibration of RF transmitter arrays. Magn Reson Med 2009;61: 1480–1488.
17. Van de Moortele PF, Akgun C, Adriany G, et al. B(1) destructive interferences and spatial phase patterns at 7 T with a head transceiver array coil. Magn Reson Med 2005;54:1503–1518.
18. Vaughan JT, DelaBarre L, Snyder CJ, et al. 9.4T human MRI: preliminary results. Magn Reson Med 2006;56:1274–1282.
19. Ishimori Y, Yamada K, Kimura H, et al. Correction of inhomogeneous RF field using multiple SPGR signals for high-field spin-echo MRI. Magn Reson Med 2007;6:67–73.
20. Pennell DJ, Sechtem UP, Higgins CB, et al. Clinical indications for cardiovascular magnetic resonance (CMR): consensus panel report. Eur Heart J 2004;25:1940–1965.